Research Report

2008-16

Analytical Solution for Cogging Torque in Surface Permanent-Maget Motors Using Conformal Mapping

D. Zarko*, D. Ban*, T.A. Lipo**

*University of Zagreb
Zagreb, Croatia

**University of Wisconsin-Madison
Madison, WI, USA

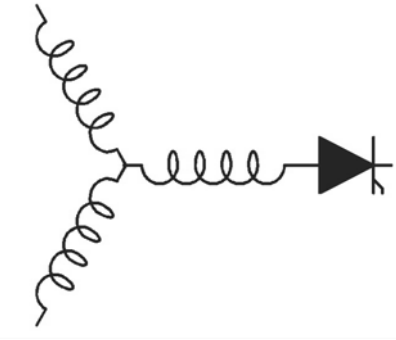

Wisconsin
Electric
Machines &
Power
Electronics
Consortium

University of Wisconsin-Madison
College of Engineering
Wisconsin Power Electronics Research Center
2559D Engineering Hall
1415 Engineering Drive
Madison WI 53706-1691

Analytical Solution for Cogging Torque in Surface Permanent-Magnet Motors Using Conformal Mapping

Damir Žarko[1], Drago Ban[1], and Thomas A. Lipo[2], *Fellow, IEEE*

[1]Faculty of Electrical Engineering and Computing, Department of Electrical Machines, Drives and Automation, University of Zagreb, HR-10000 Zagreb, Croatia

[2]Department of Electrical and Computer Engineering, University of Wisconsin-Madison, Madison WI 53706-1691 USA

We present an analytical method for the calculation of cogging torque in surface permanent-magnet (PM) motors. The cogging torque is calculated by integrating the Maxwell stress tensor inside the air gap. The principle of complex relative air-gap permeance derived from conformal transformation of the slot geometry is used to take into account the effect of slotting and to calculate the radial and tangential components of the air-gap flux density required for integration of the tangential component of the Maxwell stress tensor. We implemented the proposed analytical solution on a 7-kW four-pole surface PM motor and compared the results with finite-element solutions. We present an example of finding the optimal magnet angular span to yield minimum cogging torque as an example of the effectiveness of the method.

Index Terms—**Air-gap permeance, cogging torque, magnetic fields, permanent-magnet motors.**

I. Introduction

THE cogging torque is a well-known phenomenon which occurs in permanent-magnet motors. It is caused by the tendency of the rotor to line up with the stator in a particular direction where the permeance of the magnetic circuit seen by the permanent magnets is maximized. Together with the ripple torque caused by the mismatch between the back-electromotive force (back-EMF) and the current waveforms it represents torque pulsations which are highly undesirable in some applications, such as servo drives or electric steering.

A significant number of publications on cogging torque calculation and minimization can be found. Numerous methods, some of which are mentioned later in the paper, have been developed for cogging torque minimization, and new ones are still emerging. Therefore, the ability to calculate the cogging torque and predict correctly the effect that cogging torque minimization techniques have on its waveform and magnitude is important.

Although accurate field and torque calculations in electrical machines can be carried out using the finite-element method (FEM), numerical methods are, in general, more time consuming and do not provide closed form solutions. Alternatively, analytical field solutions can be commonly expressed in the form of Fourier series which makes them more flexible as a design tool for predicting the motor performance. This is crucial when optimization is involved in motor design, because it requires numerous repetitive calculations before reaching the optimal solution, which can be very time-consuming.

There are three basic approaches to the analytical calculation of cogging torque. One approach is to calculate the torque as a derivative of co-energy inside the air gap [1]–[7]. The second approach is to integrate the lateral forces along the slot sides [8]–[12]. The third approach, which is used in this paper, is to integrate the tangential component of Maxwell stress tensor along a circular contour inside the air gap. The analytical solution of this type is difficult to find in the literature since it requires a knowledge of both the radial and tangential components of flux density inside the slotted air gap. The analytical field solutions, which can be found in the literature [3], [5], [9], [13], [14], are able to provide fairly good estimates of only the radial component of flux density and, therefore, are not suitable for cogging torque calculation using Maxwell stress approach. One of the exceptions is [15], where both flux density components in the slotted air gap were calculated analytically.

The principle of complex relative air-gap permeance presented in [11] allows one to calculate both radial and tangential components of the air-gap flux density and, hence, leads to the analytical closed-form solution for cogging torque presented in this paper, which is based on the integral of Maxwell stress tensor. The solution is given in the form of Fourier series. One of the drawbacks of the proposed solution is the fact that the calculation of the complex relative air-gap permeance requires numerical solution of a nonlinear equation, which does not make the overall cogging torque solution entirely analytical.

There are certain artifacts of conformal mapping which lead to inaccuracies of this solution when compared to the finite-element solution, the cause of which is discussed in detail. However, the effectiveness of the proposed solution for the purpose of motor design has been shown on an example of cogging torque minimization by finding the optimal magnet-arc to pole-pitch ratio.

II. Air-Gap Field Solution

The fundamental requirement for cogging torque calculation using the Maxwell stress tensor is a knowledge of the radial and tangential components of the air-gap flux density. The principle of combining the closed form solution for the air-gap flux density in a slotless surface PM motor, given by Howe and Zhu [16], and the complex relative air-gap permeance to calculate

Digital Object Identifier 10.1109/TMAG.2007.908652

Color versions of one or more of the figures in this paper are available at http://ieeexplore.ieee.org.

the air-gap field in the slotted motor has been explained in detail in [11]. Hence, in this paper the air-gap field solution will be given without detailed derivation of all the equations.

According to results presented in [11], the flux density in the slotted air gap of a surface PM motor can be written in the form

$$\begin{aligned} B_s(r,\theta,\alpha) &= B_{sr}(r,\theta,\alpha) + jB_{s\theta}(r,\theta,\alpha) \\ &= [B_r(r,\theta,\alpha) + jB_\theta(r,\theta,\alpha)] \\ &\quad \times [\lambda_a(r,\theta) - j\lambda_b(r,\theta)] \end{aligned} \tag{1}$$

where B_r and B_θ are the radial and tangential components of the flux density in the slotless air gap, and λ_a and λ_b are the real and imaginary components of the complex relative air-gap permeance. The distribution of flux density and complex permeance along a circular arc inside the air gap can both be written in the form of Fourier series

$$\begin{aligned} B_r(r,\theta,\alpha) &= \sum_n B_{rn}(r)\cos[np(\theta-\alpha)] \\ B_\theta(r,\theta,\alpha) &= \sum_k B_{\theta n}(r)\sin[np(\theta-\alpha)] \\ \lambda_a(r,\theta) &= \lambda_0(r) + \sum_m \lambda_{am}(r)\cos(mQ_s\theta) \\ \lambda_b(r,\theta) &= \sum_m \lambda_{bm}(r)\sin(mQ_s\theta) \end{aligned} \tag{2}$$

where p is the number of pole pairs, Q_s is the number of stator slots, r is the radius inside the air gap, and α is the angular position of the rotor. The rotor position α is equal to

$$\alpha = \omega_{rm}t \tag{3}$$

where ω_{rm} is the mechanical rotor speed in rad/s and t is time. The Fourier coefficients B_{rn} and $B_{\theta n}$ are calculated from [16]

$$\begin{aligned} B_{rn}(r) = &\sum_{n=1,3,5\ldots}^{\infty} \frac{B_r}{\mu_r}\frac{4}{n\pi}\sin\left(\frac{n\pi\alpha_p}{2}\right)\frac{np}{(np)^2-1} \\ &\cdot\left[\left(\frac{r}{R_s}\right)^{np-1}\left(\frac{R_m}{R_s}\right)^{np+1}+\left(\frac{R_m}{r}\right)^{np+1}\right] \\ &\times\left\{\frac{np-1+2\left(\frac{R_r}{R_m}\right)^{np+1}-(np+1)\left(\frac{R_r}{R_m}\right)^{2np}}{\frac{\mu_r+1}{\mu_r}\left[1-\left(\frac{R_r}{R_s}\right)^{2np}\right]-\frac{\mu_r-1}{\mu_r}\left[\left(\frac{R_m}{R_s}\right)^{2np}-\left(\frac{R_r}{R_m}\right)^{2np}\right]}\right\} \end{aligned} \tag{4}$$

$$\begin{aligned} B_{\theta n}(r) = &\sum_{n=1,3,5\ldots}^{\infty} \frac{B_r}{\mu_r}\frac{4}{n\pi}\sin\left(\frac{n\pi\alpha_p}{2}\right)\frac{np}{(np)^2-1} \\ &\cdot\left[-\left(\frac{r}{R_s}\right)^{np-1}\left(\frac{R_m}{R_s}\right)^{np+1}+\left(\frac{R_m}{r}\right)^{np+1}\right] \\ &\times\left\{\frac{np-1+2\left(\frac{R_r}{R_m}\right)^{np+1}-(np+1)\left(\frac{R_r}{R_m}\right)^{2np}}{\frac{\mu_r+1}{\mu_r}\left[1-\left(\frac{R_r}{R_s}\right)^{2np}\right]-\frac{\mu_r-1}{\mu_r}\left[\left(\frac{R_m}{R_s}\right)^{2np}-\left(\frac{R_r}{R_m}\right)^{2np}\right]}\right\} \end{aligned} \tag{5}$$

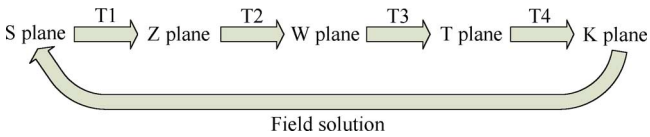

Fig. 1. Basic steps required for finding the field solution in the slotted air gap based on conformal mapping of the slot opening.

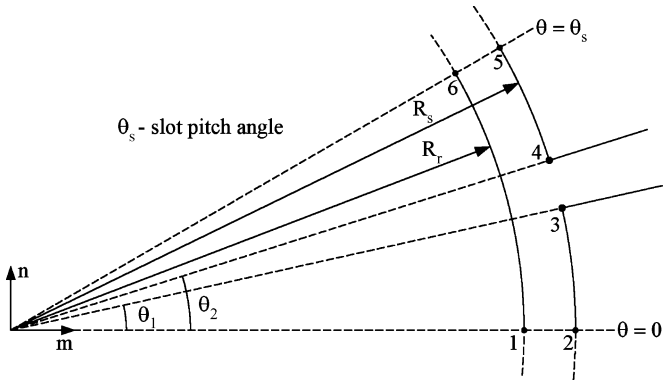

Fig. 2. Single infinitely deep slot opening in the S plane.

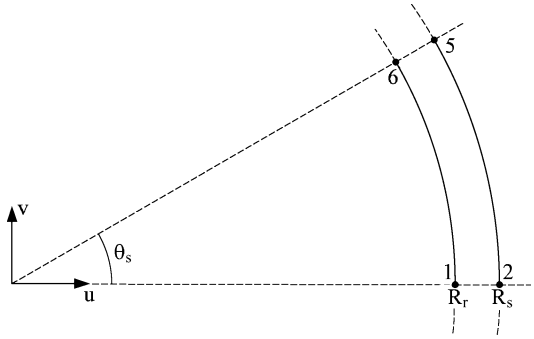

Fig. 3. Slot opening in the K plane (slotless air gap).

where B_r is the magnet remanence, μ_r is the relative recoil permeability, α_p is the magnet-arc to pole-pitch ratio, R_m is the radius at the magnet surface, R_s is the radius at the stator inner surface, and R_r is the radius at the rotor core outer surface.

The complex relative air-gap permeance is obtained by transforming the actual slotted air gap into a slotless air gap using four conformal transformations. This is shown in Fig. 1. The S plane contains the original slot geometry (Fig. 2), and the K plane contains the slotless air gap (Fig. 3), while Z, W, and T planes are used for intermediate transformations.

The individual transformations between the planes can be written in the form of partial differential equations [11]

$$\begin{aligned} &\mathrm{T1}: \frac{\partial z}{\partial s} = \frac{1}{s} \\ &\mathrm{T2}: \frac{\partial w}{\partial z} = -j\frac{\pi}{g'}\frac{(w-1)w}{(w-a)^{\frac{1}{2}}(w-b)^{\frac{1}{2}}} \\ &\mathrm{T3}: \frac{\partial t}{\partial w} = j\frac{g'}{\pi}\frac{1}{w} \\ &\mathrm{T4}: \frac{\partial k}{\partial t} = e^t = e^{\ln k} = k \end{aligned} \tag{6}$$

where

$$b = \left[\frac{b_o'}{2g'} + \sqrt{\left(\frac{b_o'}{2g'}\right)^2 + 1}\right]^2, \quad a = \frac{1}{b}$$
$$g' = \ln\left(\frac{R_s}{R_r}\right)$$
$$b_o' = \theta_2 - \theta_1.$$

The coefficients a and b represent the values of w at the corner points of the slot (points 3 and 4 in Fig. 2). The meaning of angles θ_1 and θ_2 is obvious from Fig. 2. The transformations of coordinates after solving (6) are given by

$$\begin{aligned}
&\mathrm{T1}: s = e^z \\
&\mathrm{T2}: z = j\frac{g'}{\pi}\left[\ln\left|\frac{1+p}{1-p}\right| - \ln\left|\frac{b+p}{b-p}\right| - \frac{2(b-1)}{\sqrt{b}}\tan^{-1}\frac{p}{\sqrt{b}}\right] \\
&\qquad + \ln(R_s) + j\theta_2, \left(p = \sqrt{\frac{w-b}{w-a}}\right) \\
&\mathrm{T3}: t = j\frac{g'}{\pi}\ln(w) + \ln(R_s) + j\frac{\theta_s}{2} \\
&\mathrm{T4}: k = e^t.
\end{aligned} \tag{7}$$

The link between flux density in the S and K planes is given by

$$B_s = B_k\left(\frac{\partial k}{\partial s}\right)^* = B_k\left(\frac{\partial k}{\partial t}\frac{\partial t}{\partial w}\frac{\partial w}{\partial z}\frac{\partial z}{\partial s}\right)^*. \tag{8}$$

Substituting (6) into (8) yields

$$\begin{aligned}
B_s &= B_k\left[\frac{k}{s}\frac{(w-1)}{(w-a)^{\frac{1}{2}}(w-b)^{\frac{1}{2}}}\right]^* \\
&= B_k\lambda^* = (B_r + jB_\theta)(\lambda_a + j\lambda_b)^*
\end{aligned} \tag{9}$$

where λ^* represents the complex conjugate of the complex relative air-gap permeance with λ_a and λ_b as its real and imaginary parts. The flux density B_k with its real and imaginary parts B_r and B_θ represents the field solution in the slotless air gap given by (2), (4), and (5). Since k is a function of t, which in turn is a function of w, and s is the known coordinate in the actual geometry, which is also a function of w, the complex permeance λ is indirectly a nonlinear function of w as well. For each known coordinate s in the air gap of a motor given by radius r and angle $\theta (s = r\cos\theta + jr\sin\theta)$, a value of λ can be found using (7) and (9). Unfortunately, transformation $T2$ in (7) is a nonlinear equation. In order to calculate the complex permeance λ, the coordinate w must be calculated from $T2$ using some numerical method for solving nonlinear equations. The Fourier coefficients λ_0, λ_{am}, and λ_{bm} in (2) are calculated from the real and imaginary parts of λ at geometric points along a circular arc at radius $R_m \le r \le R_s$ and an angular span of one slot-pitch using the discrete Fourier transform.

Examples of the field solution in the middle of the air gap ($r = R_s - g/2$) for the four-pole surface PM motor (Fig. 4), with parameters given in Table I, are shown in Figs. 5–7. The field solution is given for the case when the centerline of the magnet is aligned with the centerline of the slot opening. The analytically calculated flux density shows good agreement with finite-element solution for both radial and tangential components.

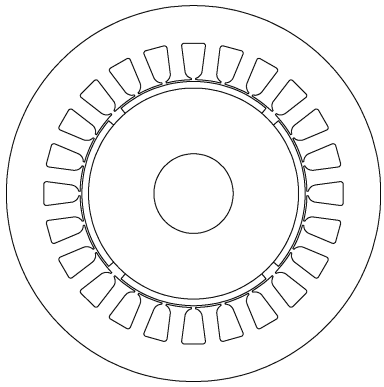

Fig. 4. Cross section of the four-pole surface PM motor.

TABLE I
PARAMETERS OF THE 24-SLOT FOUR-POLE SURFACE PM MOTOR WITH IEC FRAME SIZE 112

Parameter	*Symbol*	*Value*	*Unit*
Rated power	P_r	7	kW
Rated voltage	V_r	400	V
Rated speed	n_r	3000	rpm
Pole number	$2p$	4	–
Slot number	Q_s	24	–
Magnet-arc to pole-pitch ratio	α_p	0.9	–
Air-gap length	g	0.8	mm
Magnet radial thickness	l_m	3	mm
Slot opening width	b_o	2.0	mm
Slot opening depth	d_o	0.6	mm
Radius of the rotor surface	R_r	47.7	mm
Radius of the magnet surface	R_m	50.7	mm
Stator inner radius	R_s	51.5	mm
Stator outer radius	R_o	85.0	mm
Stack length	l_a	210.0	mm
Magnet remanence	B_r	1.2	T
Relative recoil permeability	μ_r	1.04	–
Magnetization type	–	radial	–

III. COGGING TORQUE CALCULATION BASED ON MAXWELL STRESS THEORY

According to Maxwell's theory, it is possible to calculate the total force on a rigid body placed in the electromagnetic field by integrating the magnetic stress on the closed surface around the body. The magnetic stress vector, i.e., the force per unit surface, is given by [17]

$$\vec{t}_m = \left(\vec{n}\cdot\frac{\vec{B}}{\mu_0}\right)\vec{B} - \vec{n}\frac{1}{2}\frac{|\vec{B}|^2}{\mu_0} \tag{10}$$

where $\vec{n}$ is the surface normal vector and $\vec{B}$ is the flux density vector on the surface of the body. It is clear from (10) that the stress vector consists of two components. One component of the vector $\vec{t}_m$ is in the direction of the field $\vec{B}$ and the other is perpendicular to the surface and directed towards it, as shown in Fig. 8.

The surface which encloses the rotor of a surface PM motor is in the shape of a cylinder placed entirely inside the air gap.

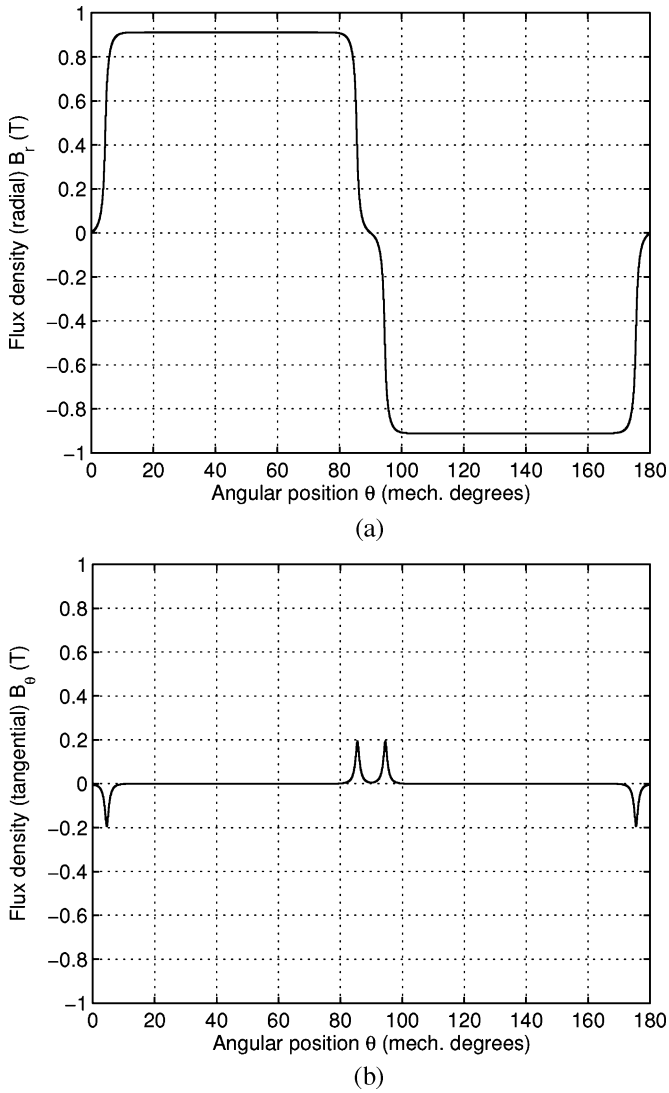

Fig. 5. Waveforms of the flux density in the middle of the air gap of a slotless surface PM motor. (a) Radial component. (b) Tangential component.

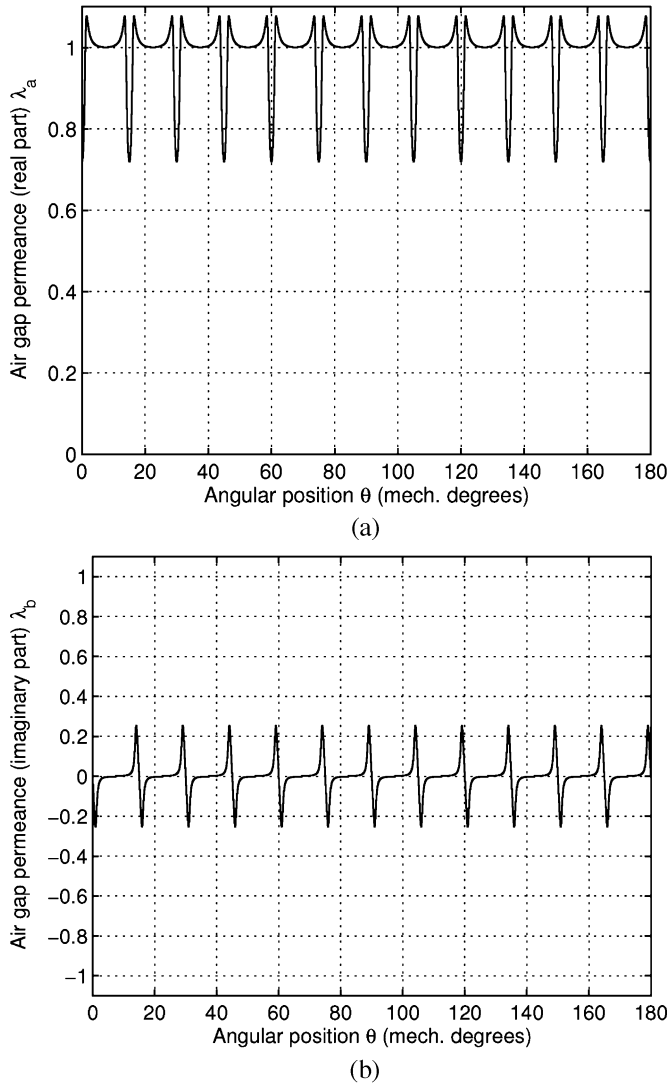

Fig. 6. Waveforms of the complex relative air-gap permeance in the middle of the air gap of a slotted surface PM motor. (a) Real component. (b) Imaginary component.

In that case the surface normal vector will be equal to the unit length vector in the radial direction, i.e.,

$$\vec{n} = \vec{a}_r. \tag{11}$$

The flux density vector $\vec{B}$ will have radial and tangential components, and can be written in the form

$$\vec{B} = B_r\vec{a}_r + B_\theta\vec{a}_\theta. \tag{12}$$

Substituting (11) and (12) into (10) yields

$$\begin{aligned}\vec{t}_m &= \frac{1}{\mu_0}\left[\vec{a}_r \cdot (B_r\vec{a}_r + B_\theta\vec{a}_\theta)\right](B_r\vec{a}_r + B_\theta\vec{a}_\theta) - \vec{a}_r\frac{1}{2}\frac{|\vec{B}|^2}{\mu_0} \\ &= \frac{1}{\mu_0}B_r(B_r\vec{a}_r + B_\theta\vec{a}_\theta) - \vec{a}_r\frac{1}{2}\frac{|\vec{B}|^2}{\mu_0} \\ &= \frac{1}{\mu_0}\left(B_r^2 - \frac{1}{2}|\vec{B}|^2\right)\vec{a}_r + \frac{1}{\mu_0}B_rB_\theta\vec{a}_\theta. \end{aligned} \tag{13}$$

The tangential component of the magnetic stress vector is of particular interest for torque calculations. The total tangential force on the rotor is equal to the surface integral of the tangential component of the stress vector. Hence, the motor torque is equal to the total force multiplied by the radius of the cylindrical integration surface. If it is assumed that the field is uniform in the axial direction, then the surface integral becomes a line integral multiplied by the stack length of the machine. The torque equation in the integral form can then be written as

$$T = \frac{1}{\mu_0}l_a r^2 \int_0^{2\pi} B_{sr}(r,\theta,\alpha)B_{s\theta}(r,\theta,\alpha)\mathrm{d}\theta \tag{14}$$

where μ_0 is the permeability of vacuum, l_a is the stack length of the machine, r is the radius of the integration surface, B_{sr} is the radial and $B_{s\theta}$ is the tangential component of the flux density at radius r.

The radius inside the air gap at which the integration surface is positioned is arbitrary, but for calculation purposes it can be

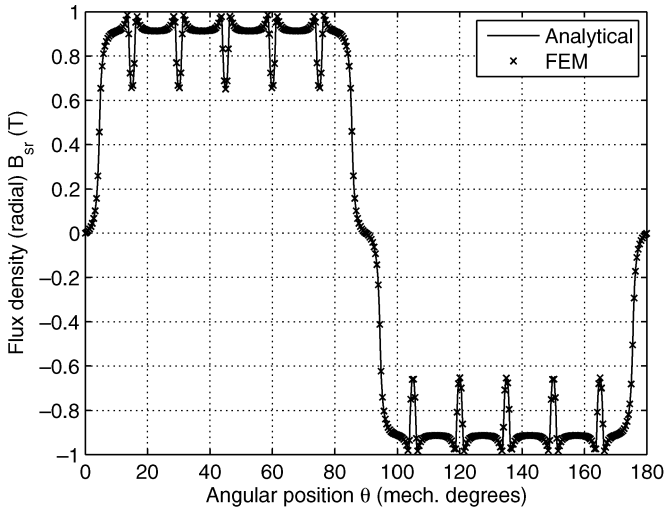

Fig. 7. Waveforms of the flux density in the middle of the air gap of a slotted surface PM motor. (a) Radial component. (b) Tangential component.

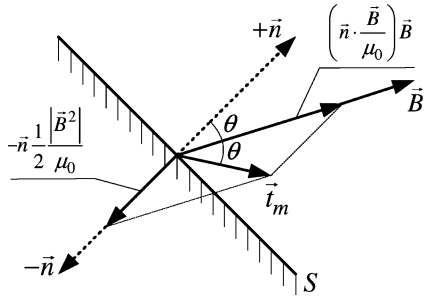

Fig. 8. Relationship between vectors $\vec{n}$, $\vec{B}$, and $\vec{t}_m$.

problematic if the surface is placed too close to the stator inner surface. The problem occurs at the tooth tips because at those points the complex relative air-gap permeability λ has an infinite value. For a simple slot opening, the tooth tips are located at the points where $w = a$ and $w = b$. It is apparent from (9) that at these points λ is infinite. To avoid numerical problems of dealing with infinite numbers or with very large values of λ at a radius very close to the stator surface, the analysis will be done in the middle of the air gap at the radius $r = R_s - g/2$ at which the complex permeance λ and the flux density distribution have been evaluated earlier.

At this point, the field solution in the air gap of a surface PM motor at no-load operation is known. That field solution can now be used to calculate the cogging torque by integrating the Maxwell stress vector according to (14).

According to (1) and (2), the radial and tangential components of the flux density in the slotted air gap can be written as

$$\begin{aligned} B_{sr}(r,\theta,\alpha) &= B_r(r,\theta,\alpha)\lambda_a(r,\theta) + B_\theta(r,\theta,\alpha)\lambda_b(r,\theta) \\ &= \lambda_0(r)\sum_n B_{rn}(r)\cos\left[np(\theta-\alpha)\right] \\ &+ \sum_n\sum_m B_{rn}(r)\lambda_{am}(r)\cos\left[np(\theta-\alpha)\right]\cos(mQ_s\theta) \\ &+ \sum_n\sum_m B_{\theta n}(r)\lambda_{bm}(r)\sin\left[np(\theta-\alpha)\right]\sin(mQ_s\theta) \quad (15) \\ B_{s\theta}(r,\theta,\alpha) &= B_\theta(r,\theta,\alpha)\lambda_a(r,\theta) - B_r(r,\theta,\alpha)\lambda_b(r,\theta) \\ &= \lambda_0(r)\sum_n B_{\theta n}(r)\sin\left[np(\theta-\alpha)\right] \\ &+ \sum_n\sum_m B_{\theta n}(r)\lambda_{am}(r)\sin\left[np(\theta-\alpha)\right]\cos(mQ_s\theta) \\ &- \sum_n\sum_m B_{rn}(r)\lambda_{bm}(r)\cos\left[np(\theta-\alpha)\right]\sin(mQ_s\theta). \quad (16) \end{aligned}$$

The integrand of (14) includes terms consisting of multiple sums. Using a different variable name for each sum in (15) and (16) and knowing that the Fourier coefficients in the expressions for the flux density and the complex permeance are calculated at the radius $r = R_s - g/2$, the cogging torque expression takes the form given by (17)

$$\begin{aligned} T_c(\alpha) = \frac{1}{\mu_0} l_a r^2 \Bigg\{ & \lambda_0^2 \sum_n\sum_k B_{rn}B_{\theta k}\int_0^{2\pi}\cos\left[np(\theta-\alpha)\right] \\ & \times \sin\left[kp(\theta-\alpha)\right]\mathrm{d}\theta \\ & + \lambda_0 \sum_n\sum_k\sum_h B_{rn}B_{\theta k}\lambda_{ah} \\ & \times \int_0^{2\pi}\cos\left[np(\theta-\alpha)\right]\sin\left[kp(\theta-\alpha)\right] \\ & \times \cos(hQ_s\theta)\mathrm{d}\theta \\ & - \lambda_0 \sum_n\sum_k\sum_h B_{rn}B_{rk}\lambda_{bh} \\ & \times \int_0^{2\pi}\cos\left[np(\theta-\alpha)\right]\cos\left[kp(\theta-\alpha)\right] \\ & \times \sin(hQ_s\theta)\mathrm{d}\theta \\ & + \lambda_0 \sum_n\sum_k\sum_m B_{rn}B_{\theta k}\lambda_{am} \\ & \times \int_0^{2\pi}\cos\left[np(\theta-\alpha)\right]\sin\left[kp(\theta-\alpha)\right] \\ & \times \cos(mQ_s\theta)\mathrm{d}\theta \end{aligned}$$

$$
\begin{aligned}
&+\lambda_0 \sum_n \sum_k \sum_m B_{\theta n} B_{\theta k} \lambda_{bm} \\
&\times \int_0^{2\pi} \sin\left[np(\theta-\alpha)\right] \sin\left[kp(\theta-\alpha)\right] \\
&\times \sin(mQ_s\theta)\mathrm{d}\theta \\
&+\sum_n \sum_k \sum_m \sum_h B_{rn} B_{\theta k} \lambda_{am} \lambda_{ah} \\
&\times \int_0^{2\pi} \cos\left[np(\theta-\alpha)\right] \sin\left[kp(\theta-\alpha)\right] \\
&\times \cos(mQ_s\theta)\cos(hQ_s\theta)\mathrm{d}\theta \\
&+\sum_n \sum_k \sum_m \sum_h B_{\theta n} B_{\theta k} \lambda_{bm} \lambda_{ah} \\
&\times \int_0^{2\pi} \sin\left[np(\theta-\alpha)\right] \sin\left[kp(\theta-\alpha)\right] \\
&\times \sin(mQ_s\theta)\cos(hQ_s\theta)\mathrm{d}\theta \\
&-\sum_n \sum_k \sum_m \sum_h B_{rn} B_{rk} \lambda_{am} \lambda_{bh} \\
&\times \int_0^{2\pi} \cos\left[np(\theta-\alpha)\right] \cos\left[kp(\theta-\alpha)\right] \\
&\times \cos(mQ_s\theta)\sin(hQ_s\theta)\mathrm{d}\theta \\
&-\sum_n \sum_k \sum_m \sum_h B_{\theta n} B_{rk} \lambda_{bm} \lambda_{bh} \\
&\times \int_0^{2\pi} \sin\left[np(\theta-\alpha)\right] \cos\left[kp(\theta-\alpha)\right] \\
&\times \sin(mQ_s\theta)\sin(hQ_s\theta)\mathrm{d}\theta \Bigg\}. \qquad (17)
\end{aligned}
$$

The integrals in (17) will yield a result different from zero only for certain values of n, k, m, and h. One of the terms from (17) is used below as an example to show for which combinations of n, k, m, and h the integral $\int_0^{2\pi}$ will be different from zero. The integrands in (17) are expressed as the products of sine and cosine functions. Before integration, they need to be transformed into sums of sine and cosine functions using basic identities for trigonometric functions. For the second term in (17), one has

$$
\begin{aligned}
I &= \lambda_0 \sum_n \sum_k \sum_h B_{rn} B_{\theta k} \lambda_{ah} \\
&\quad \times \int_0^{2\pi} \left\{\cos\left[np(\theta-\alpha)\right] \sin\left[kp(\theta-\alpha)\right] \cos(hQ_s\theta)\right\} \mathrm{d}\theta \\
&= \lambda_0 \sum_n \sum_k \sum_h B_{rn} B_{\theta k} \lambda_{ah} \\
&\quad \times \int_0^{2\pi} \frac{1}{2} \left\{\sin\left[(kp+np)\theta-(kp+np)\alpha\right]\right. \\
&\qquad \left. +\sin\left[(kp-np)\theta-(kp-np)\alpha\right]\right\} \cos(hQ_s\theta)\mathrm{d}\theta \\
&= \lambda_0 \sum_n \sum_k \sum_h B_{rn} B_{\theta k} \lambda_{ah} \\
&\quad \times \int_0^{2\pi} \frac{1}{4} \{\sin\left[(kp+np+hQ_s)\theta-(kp+np)\alpha\right] \\
&\qquad +\sin[(kp+np-hQ_s)\theta-(kp+np)\alpha)] \\
&\qquad +\sin[(kp-np+hQ_s)\theta-(kp-np)\alpha)] \\
&\qquad +\sin[(kp-np-hQ_s)\theta-(kp-np)\alpha)]\} \,\mathrm{d}\theta. \qquad (18)
\end{aligned}
$$

It is easy to show from (18) that when

$$kp + np - hQ_s = 0$$

the value of I will be

$$I = -\sum_n \sum_k \sum_h \lambda_0 \frac{\pi}{2} B_{rn} B_{\theta k} \lambda_{ah} \sin\left[p(n+k)\alpha\right]. \qquad (19)$$

Similarly, when

$$kp - np + hQ_s = 0 \text{ or } kp - np - hQ_s = 0$$

the value of I will be

$$I = \sum_n \sum_k \sum_h \lambda_0 \frac{\pi}{2} B_{rn} B_{\theta k} \lambda_{ah} \sin\left[p(n-k)\alpha\right]. \qquad (20)$$

For all other combinations of k, n, and h, I is equal to zero. The same principle can be used for all other terms in (17). Hence, the final expression for cogging torque as a function of the rotor position is given by (21), shown on the next page.

From (7), it is apparent that transformations of coordinates between complex planes involve logarithmic functions. The transformation of the infinitely long slot sides in the S plane into a circular arc of finite length on the stator surface in the K plane is achieved by logarithmic scaling of coordinates. This transformation inevitably deforms the local space around the slot opening since it condenses an infinite space into a finite space. If the flux density needs to be calculated at a location defined by the coordinates $s = m + jn$ in the S plane, then the value of the flux density in the slotless air gap which is used in (9) needs to be evaluated at a point $k = u + jv$ in the K plane into which the point s is transformed. Note that the outline of the slot opening in Fig. 2 will be transformed into the outline of the slotless air gap in Fig. 3. However, the radial and the angular coordinates of the points in the S plane will not be exactly transformed into the same coordinates of the points in the K plane. For instance, if the field distribution in the slotted air gap needs to be evaluated along a circular line with radius r where $s = re^{j\theta}$ and $R_m < r < R_s$, then the field distribution in the K plane needs to be evaluated along a contour into which the circular arc is transformed. For the previously used four-pole surface PM motor the circular arc located in the middle of the air gap, with the radius $r = R_s - g/2$ and an angular span of one slot pitch, and the contour in the K plane into which this arc is transformed have been compared in Fig. 9. If the points in the S plane are given in the form $s = r_s e^{j\theta_s}$ and the transformed points in the K plane are given in the form $k = r_k e^{j\theta_k}$, then Fig. 9(a) shows the ratio of the radii r_k/r_s

$$
\begin{aligned}
&kp+np-mQ_s=0\\
&T_c(\alpha)=\frac{1}{\mu_0}l_a r^2\sum_n\sum_k\sum_m\lambda_0\frac{\pi}{2}(-2B_{rn}B_{\theta k}\lambda_{am}-B_{\theta n}B_{\theta k}\lambda_{bm}-B_{rn}B_{rk}\lambda_{bm})\sin[p(n+k)\alpha]\\
&kp-np+mQ_s=0\\
&T_c(\alpha)=\frac{1}{\mu_0}l_a r^2\sum_n\sum_k\sum_m\lambda_0\frac{\pi}{2}(2B_{rn}B_{\theta k}\lambda_{am}+B_{\theta n}B_{\theta k}\lambda_{bm}-B_{rn}B_{rk}\lambda_{bm})\sin[p(n-k)\alpha]\\
&kp-np-mQ_s=0\\
&T_c(\alpha)=\frac{1}{\mu_0}l_a r^2\sum_n\sum_k\sum_m\lambda_0\frac{\pi}{2}(2B_{rn}B_{\theta k}\lambda_{am}-B_{\theta n}B_{\theta k}\lambda_{bm}+B_{rn}B_{rk}\lambda_{bm})\sin[p(n-k)\alpha]\\
&kp+np+mQ_s-hQ_s=0\\
&T_c(\alpha)=\frac{1}{\mu_0}l_a r^2\sum_n\sum_k\sum_m\sum_h\frac{\pi}{4}(-B_{rn}B_{rk}\lambda_{am}\lambda_{bh}-B_{rn}B_{\theta k}\lambda_{am}\lambda_{ah}+B_{\theta n}B_{\theta k}\lambda_{bm}\lambda_{ah}+B_{\theta n}B_{rk}\lambda_{bm}\lambda_{bh})\\
&\qquad\times\sin[p(n+k)\alpha]\\
&kp+np-mQ_s+hQ_s=0\\
&T_c(\alpha)=\frac{1}{\mu_0}l_a r^2\sum_n\sum_k\sum_m\sum_h\frac{\pi}{4}(B_{rn}B_{rk}\lambda_{am}\lambda_{bh}-B_{rn}B_{\theta k}\lambda_{am}\lambda_{ah}-B_{\theta n}B_{\theta k}\lambda_{bm}\lambda_{ah}+B_{\theta n}B_{rk}\lambda_{bm}\lambda_{bh})\\
&\qquad\times\sin[p(n+k)\alpha]\\
&kp+np-mQ_s-hQ_s=0\\
&T_c(\alpha)=\frac{1}{\mu_0}l_a r^2\sum_n\sum_k\sum_m\sum_h\frac{\pi}{4}(-B_{rn}B_{rk}\lambda_{am}\lambda_{bh}-B_{rn}B_{\theta k}\lambda_{am}\lambda_{ah}-B_{\theta n}B_{\theta k}\lambda_{bm}\lambda_{ah}-B_{\theta n}B_{rk}\lambda_{bm}\lambda_{bh})\\
&\qquad\times\sin[p(n+k)\alpha]\\
&kp-np+mQ_s+hQ_s=0\\
&T_c(\alpha)=\frac{1}{\mu_0}l_a r^2\sum_n\sum_k\sum_m\sum_h\frac{\pi}{4}(-B_{rn}B_{rk}\lambda_{am}\lambda_{bh}+B_{rn}B_{\theta k}\lambda_{am}\lambda_{ah}+B_{\theta n}B_{\theta k}\lambda_{bm}\lambda_{ah}-B_{\theta n}B_{rk}\lambda_{bm}\lambda_{bh})\\
&\qquad\times\sin[p(n-k)\alpha]\\
&kp-np+mQ_s-hQ_s=0\\
&T_c(\alpha)=\frac{1}{\mu_0}l_a r^2\sum_n\sum_k\sum_m\sum_h\frac{\pi}{4}(B_{rn}B_{rk}\lambda_{am}\lambda_{bh}+B_{rn}B_{\theta k}\lambda_{am}\lambda_{ah}+B_{\theta n}B_{\theta k}\lambda_{bm}\lambda_{ah}+B_{\theta n}B_{rk}\lambda_{bm}\lambda_{bh})\\
&\qquad\times\sin[p(n-k)\alpha]\\
&kp-np-mQ_s+hQ_s=0\\
&T_c(\alpha)=\frac{1}{\mu_0}l_a r^2\sum_n\sum_k\sum_m\sum_h\frac{\pi}{4}(-B_{rn}B_{rk}\lambda_{am}\lambda_{bh}+B_{rn}B_{\theta k}\lambda_{am}\lambda_{ah}-B_{\theta n}B_{\theta k}\lambda_{bm}\lambda_{ah}+B_{\theta n}B_{rk}\lambda_{bm}\lambda_{bh})\\
&\qquad\times\sin[p(n-k)\alpha]\\
&kp-np-mQ_s-hQ_s=0\\
&T_c(\alpha)=\frac{1}{\mu_0}l_a r^2\sum_n\sum_k\sum_m\sum_h\frac{\pi}{4}(B_{rn}B_{rk}\lambda_{am}\lambda_{bh}+B_{rn}B_{\theta k}\lambda_{am}\lambda_{ah}-B_{\theta n}B_{\theta k}\lambda_{bm}\lambda_{ah}-B_{\theta n}B_{rk}\lambda_{bm}\lambda_{bh})\\
&\qquad\times\sin[p(n-k)\alpha]
\end{aligned}
\tag{21}
$$

and Fig. 9(b) shows the angular displacement $\theta_k-\theta_s$. It is apparent that the transformed line in the K plane is very close to the circular arc in the S plane. However, if the locations of the points in the K plane at which the flux density is to be calculated were adjusted to compensate the difference between the circular arc in the S plane and the transformed curve in the K plane, then at each rotor position a new set of Fourier coefficients for the field solution in the slotless air gap, given by Howe and Zhu in [16], would have to be calculated. Hence, in order to simplify our solution, an approximation is made in which it is assumed that the transformed line in the K plane is also a circular arc with the same radial and angular coordinates as the original arc in the S plane

In addition, conformal mapping also slightly deforms the shape of the magnets in the K plane. Therefore, a similar approximation has also been made assuming that the magnets will retain their original shape as in the S plane to simplify the field calculations. The attempt to compensate the deformation of the magnet shape and improve the accuracy of the cogging torque solution would be very difficult, since the field solution in the slotless air gap [16] assumes that magnet has a shape of a circular arc. In addition, the deformation of the magnet shape

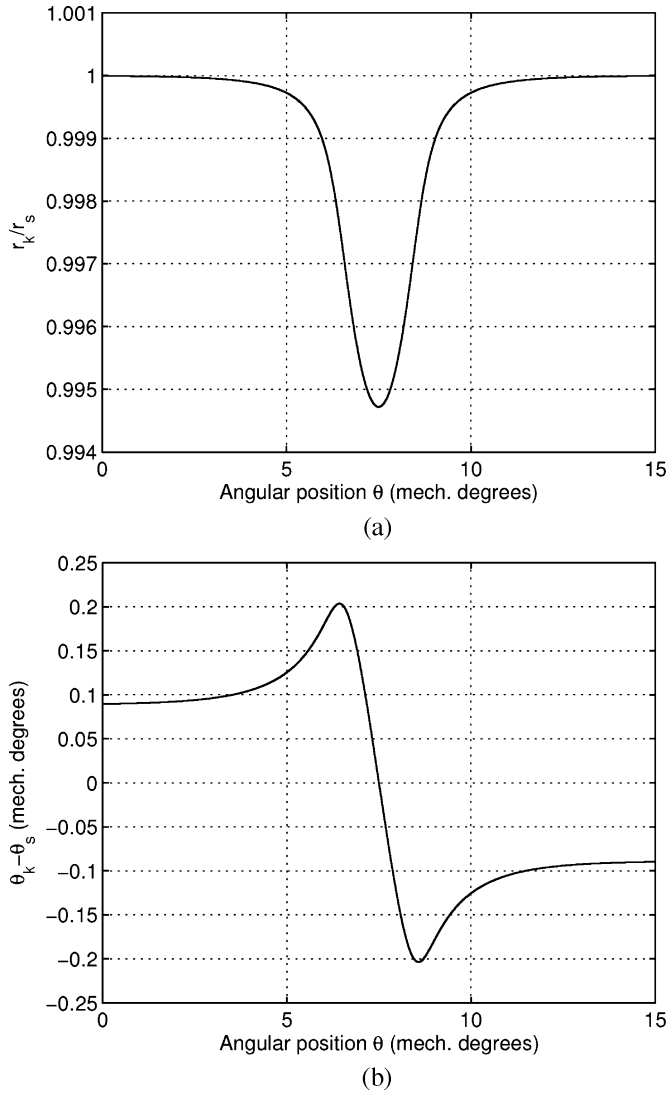

Fig. 9. Comparison of the circular arc in the middle of the air gap of a four-pole surface PM motor extending one slot pitch in the S plane and its transformed shape in the K plane. (a) Ratio r_k/r_s. (b) Angular displacement $\theta_k - \theta_s$.

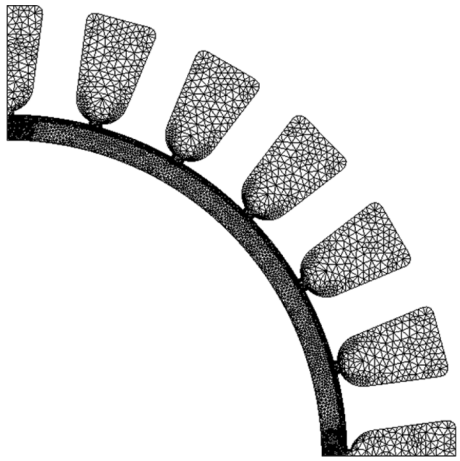

Fig. 10. Meshed finite-element model of the four pole motor.

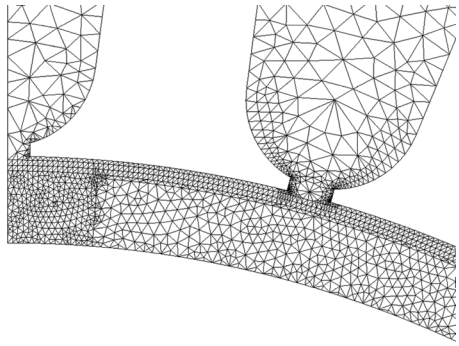

Fig. 11. Enlarged detail of the finite-element mesh in the vicinity of the slot opening and the magnet edge.

due to conformal mapping is not stationary because magnets rotate with respect to the slot openings and, hence, in each time instant different portions of the magnet surface are affected by the presence of slot openings.

Since interaction between the magnet edges and the slot opening is crucial for cogging torque production, any errors in the field solution in that sensitive area originating from spatial deformations due to conformal mapping affect the cogging torque solution as well. The negative influence of these spatial deformations will become obvious from the comparison of analytical and numerical cogging torque solutions shown later in the paper.

The cogging torque for the four-pole surface PM motor has been calculated using (21) and using the finite-element method. Two major approximations mentioned earlier were used when solving (21):

— a circular arc in the air gap in the S plane is transformed into an identical circular arc in the K plane;

— the shape of the magnet in the K plane is identical to the actual shape of the magnet in the S plane (arc-shaped with constant thickness and radial magnetization).

For the FE solution, the time-stepping transient method with moving air gap has been used. Since conformal mapping inherently assumes that the iron is infinitely permeable, for better comparison of analytical and numerical results the same assumption has been made in the FE simulation. In order to reduce the size of the FE model and the computational effort, the infinitely permeable iron was replaced with the Neumann boundary condition. Fig. 10 shows the meshed FE model with second-order elements. Fig. 11 shows an enlarged detail of the mesh in the vicinity of the slot opening, which is the region that requires fine discretization for cogging torque calculation. The mesh size has been adjusted using adaptive solver to reduce errors in the critical areas, namely the tooth tips. The cogging torque is evaluated at 60 consecutive rotor positions using virtual work method. The analytical and numerical solutions are compared in Fig. 12.

An obvious problem with the analytical solution is that it results in higher peak values of cogging torque, which is caused by spatial deformations and the approximations we used. To confirm the consistency of such results, another comparison of analytically and numerically calculated cogging torque waveforms

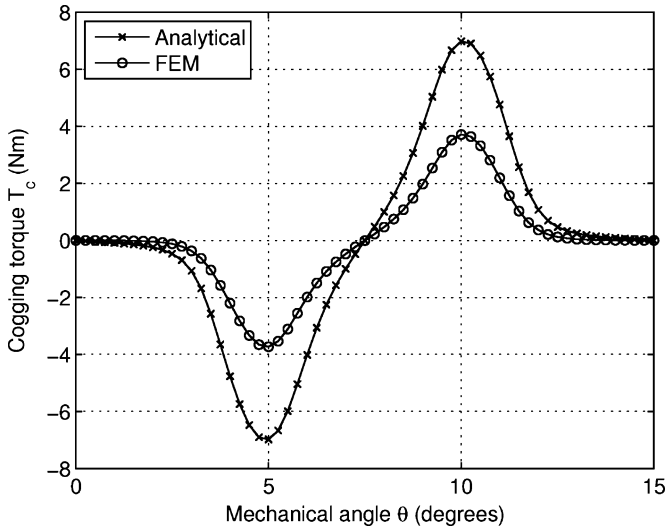

Fig. 12. Comparison of cogging torque waveforms for the four-pole motor calculated analytically and numerically using FE method.

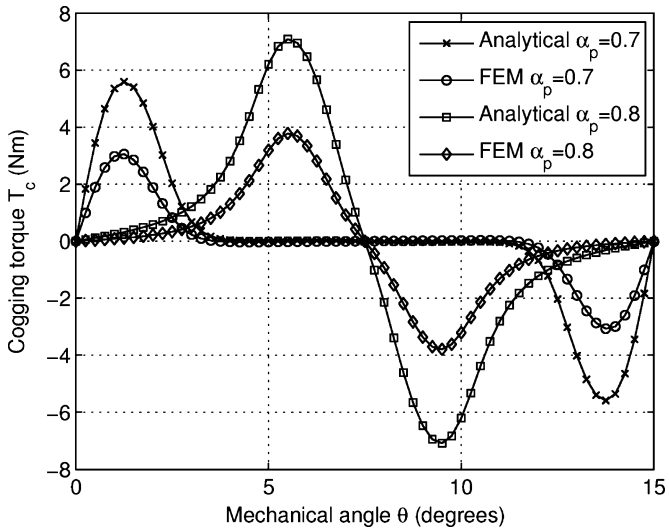

Fig. 13. Comparison of cogging torque waveforms for the four-pole motor calculated analytically and numerically for two different magnet-arc to pole-pitch ratios.

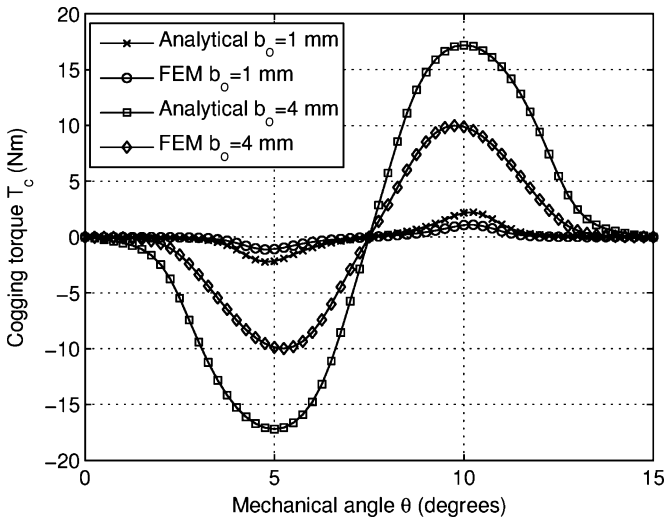

Fig. 14. Comparison of cogging torque waveforms for the four-pole motor calculated analytically and numerically for two different widths of the slot opening.

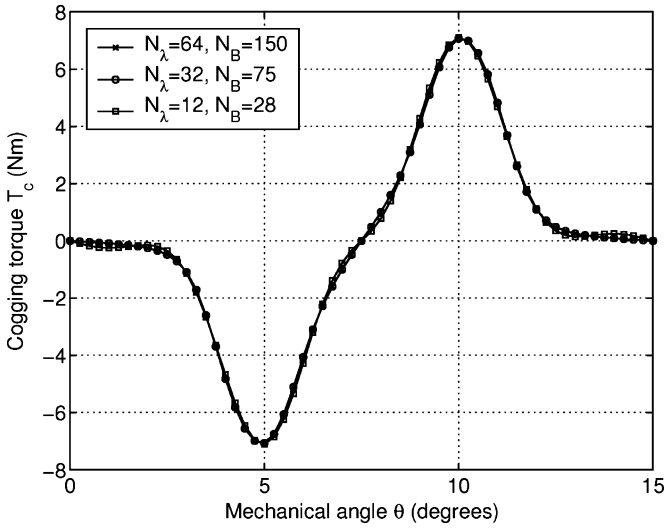

Fig. 15. Comparison of cogging torque waveforms calculated analytically for $\alpha_p = 0.9$ with different numbers of terms used in the Fourier series for the relative air-gap permeance (N_λ) and the flux density in the slotless air gap (N_B).

has been made in Fig. 13 for two different values of magnet pole-arc to pole-pitch ratio ($\alpha_p = 0.7$, $\alpha_p = 0.8$).

The cogging torque waveform is also affected by the width of the slot opening with respect to the length of the air gap. In our case, the width of the slot opening is 2 mm, and the total air gap length is 3.8 mm (air+magnet). The cogging torque waveforms have also been calculated analytically and numerically for the slot opening widths of 1 and 4 mm. The results are compared in Fig. 14. In this case, the difference in magnitude between analytically and numerically calculated waveforms is also present. Nevertheless, both analytically calculated waveforms are properly scaled, i.e., their relative deviations from the numerical results are practically the same.

The cogging torque waveforms in Figs. 12–14 were calculated using 64 terms in the Fourier series for the complex relative air-gap permeance and 150 terms for the flux density in the slotless air gap. However, the numbers of terms which are required to achieve acceptable accuracy can be significantly smaller, as indicated in Fig. 15.

According to Maxwell stress theory, the same cogging torque waveform should be calculated regardless of the location of the integration contour as long as it is located inside the air gap. To show that our cogging torque solution is consistent with this theory, the cogging torque has also been calculated at two other radii, one closer to the stator surface ($r = R_s - 0.1g$) and another closer to the magnet surface ($r = R_s - 0.9g$). The radial and tangential components of the flux density in the slotted air gap at these two radii are shown in Figs. 16 and 17. The cogging torque waveforms calculated at all three radii inside the air gap are compared in Fig. 18. It is apparent from Fig. 18 and Figs. 16 and 17 that although the field solutions at these radii differ, the cogging torque waveforms are practically the same.

It is apparent from these results that the analytical solution is able to correctly predict the effect which motor geometry has on

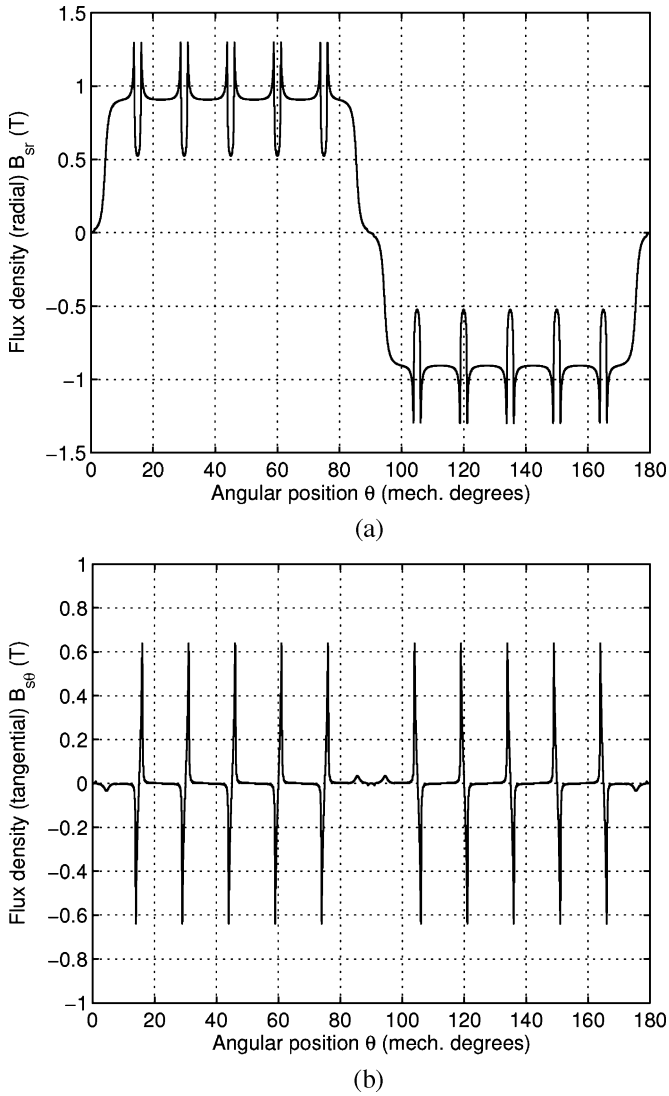

Fig. 16. Waveforms of the flux density in the air gap of a slotted surface PM motor at the radius $r = R_s - 0.1g$. (a) Radial component. (b) Tangential component.

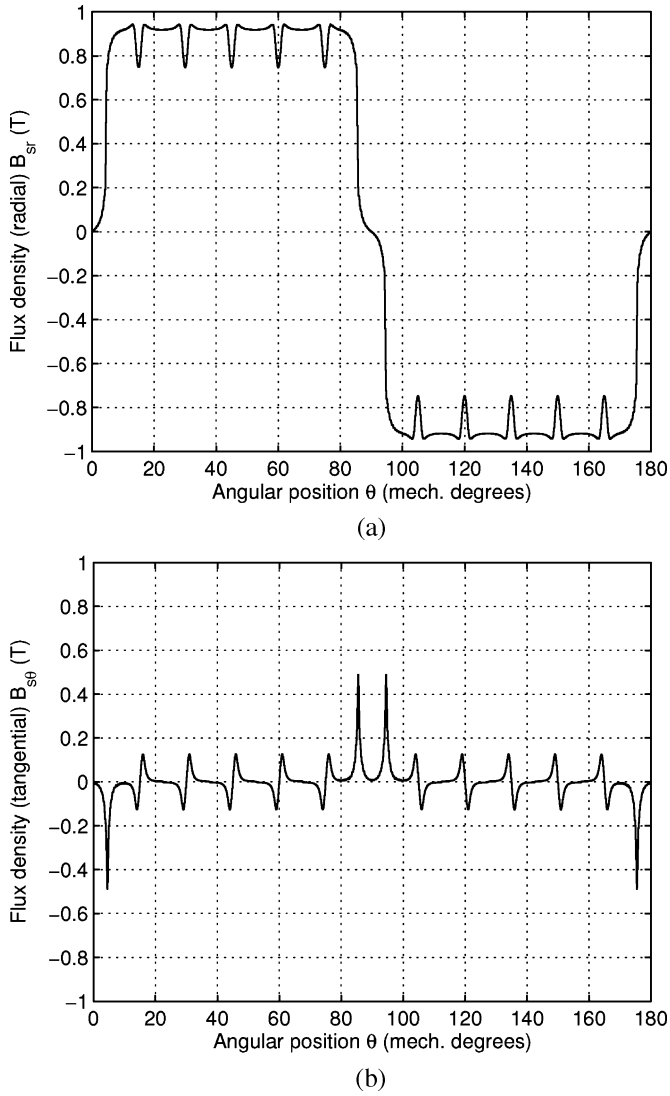

Fig. 17. Waveforms of the flux density in the air gap of a slotted surface PM motor at the radius $r = R_s - 0.9g$. (a) Radial component. (b) Tangential component.

the harmonic content of the cogging torque, both in terms of its shape and magnitude, and that it is consistent with the Maxwell stress theory. However, the problem of inaccuracy in terms of magnitude, if FE solution is taken as a reference for accuracy, remains.

Nevertheless, the analytical cogging torque solution presented in this paper is capable of capturing correctly all the effects which slot/pole combinations, size of the slot opening, air-gap length and magnet dimensions and properties have on the cogging torque waveform and magnitude. In spite of noticed differences in the magnitude of the cogging torque obtained analytically and numerically, this analytical solution can be effectively used in an analysis which involves comparison between a large number of different motor designs, which is the case when optimization is used for motor design. To support this claim, in the following section the Differential Evolution (DE) optimization method [18], [19] combined with our analytical cogging torque solution will be used to find correctly the magnet-arc to pole-pitch ratio which yields minimum cogging torque.

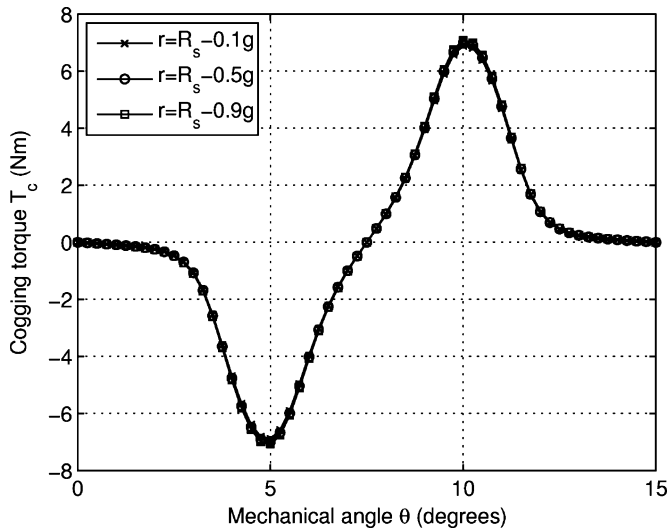

Fig. 18. Comparison of cogging torque waveforms for the four-pole motor calculated analytically at three different radii inside the air gap.

IV. Example of Implementation of Analytical Cogging Torque Solution

There are many known cogging torque minimization techniques. Adjusting the magnet-arc to pole-pitch ratio α_p is one of the simplest methods which will be used here to show the effectiveness of the presented analytical cogging torque solution. Zhu and Howe [20] showed that the optimum value of α_p is given by

$$\alpha_p = \frac{\frac{N_c}{2p} - k_1}{\frac{N_c}{2p}} + k_2, \quad k_1 = 1, 2, \ldots, Q_s - 1. \tag{22}$$

where N_c is the least common multiple between the number of slots Q_s and the number of poles $2p$, and k_2 is the factor which takes into account the fringing flux of the magnets and typically ranges from 0.01 to 0.03 depending on the air-gap length. In our case, the goal is to show that the analytical cogging torque solution presented in this paper can be successfully used to find α_p which yields minimum cogging torque and falls into the range of values defined by (22). For that purpose, the Differential Evolution optimization method has been used.

A. Description of the Differential Evolution Optimization Method

The Differential Evolution is an optimization technique capable of solving global optimization problems subject to nonlinear constraints. It operates on a population of candidate solutions and does not require a specific starting point. The population is of constant size NP. In each iteration, a new generation of solutions is created and compared to the population members of the previous generation. The process is repeated until the maximum number of generations $G_{\max}$ is reached.

A nonlinear global optimization problem can be defined as: Find the vector of parameters $\vec{x} = [x_1, x_2, \ldots, x_D], \vec{x} \in R^D$ subject to m inequality constraints and subject to D boundary constraints which will minimize the function $f(\vec{x})$.

The population of the Gth generation can be written in the form $P_G = [\vec{x}_{1,G}, \vec{x}_{2,G}, \ldots, \vec{x}_{NP,G}]$, $G = 0, \ldots, G_{\max}$. Each vector in PG contains D real parameters $\vec{x}_{i,G} = [x^i_{1,G}, x^i_{2,G}, \ldots, x^i_{D,G}]$, $i = 1, \ldots, NP$, $G = 0, \ldots, G_{\max}$

The initial population $P_{G=0}$ is generated using random values within the given boundaries which can be written in the form

$$x^i_{j,0} = \mathrm{rand}_j[0,1]\left(x^{(U)}_j - x^{(L)}_j\right) + x^{(L)}_j \qquad i = 1, \ldots, NP, \quad j = 1, \ldots, D \tag{23}$$

where $\mathrm{rand}_j[0,1]$ is the uniformly distributed random number on the interval [0,1] which is chosen anew for each j, while (U) and (L) denote the upper and lower boundaries of the vector parameters. In every generation, new candidate vectors are created by randomly sampling and combining the vectors from the previous generation in the following manner:

$$i = 1, \ldots, NP, \quad j = 1, \ldots, D, \quad G = 1, \ldots, G_{\max}$$
$$u^i_{j,G} = \begin{cases} x^{r3}_{j,G-1} + F\left(x^{r1}_{j,G-1} - x^{r2}_{j,G-1}\right) & \text{if } \mathrm{rand}_j[0,1] \le CR \text{ or } j = k \\ x^i_{j,G-1} & \text{otherwise} \end{cases} \tag{24}$$

where $F \in \langle 0, 1]$ and $CR \in [0, 1]$ are DE control parameters which are kept constant during optimization, $r_1, r_2, r_3 \in \{1, \ldots, NP\}$, $r_1 \neq r_2 \neq r_3 \neq i$ are randomly selected vectors from the previous generation, different from each other and different from the current vector with index i, and $k \in \{1, \ldots, D\}$ is a randomly chosen index which insures that at least one $u^i_{j,G}$ is different from $x^i_{j,G-1}$.

The population for the new generation P_G will be assembled from the vectors of the previous generation P_{G-1} and the candidate vectors $\vec{u}^i_G$ according to the following selection scheme:

$$i = 1, \ldots, NP, \quad G = 1, \ldots, G_{\max}$$
$$\vec{x}^i_G = \begin{cases} \vec{u}^i_G & \text{if } f\left(\vec{u}^i_G\right) \le f\left(\vec{x}^i_{G-1}\right) \\ \vec{x}^i_{G-1} & \text{otherwise.} \end{cases} \tag{25}$$

B. Definition of the Optimization Problem

The objective function which should be minimized is the peak value of cogging torque, i.e.,

$$F = \max\left[T_c(\alpha)\right], \quad 0 \le \alpha \le 15^0 (\text{mech. degrees}). \tag{26}$$

The only design variable is α_p, which is subject to constraints

$$0.7 \le \alpha_p \le 1. \tag{27}$$

All other geometric parameters of the motor are kept constant as defined in Table I. The lowest value of 0.7 was selected to avoid α_p for $k_1 = 2$, which according to (22) would fall in an interval $0.6767 \le \alpha_p \le 0.6967$. This magnet-arc would not be very suitable for practical purposes since utilization of the available space for placing the magnet within one pole-pitch would be quite poor.

The population size in the DE algorithm is set to $NP = 10$, while control parameters are $F = 0.8$, $CR = 0.9$.

C. Optimization Results

Since only one design variable is involved, the DE algorithm converged after only one iteration to 99% of the final value of α_p. After 10 iterations, the optimal value of magnet-arc to pole-pitch ratio was reached which is

$$\alpha_p = 0.8452 = \frac{5}{6} + 0.0119. \tag{28}$$

This result falls into the range of optimal values for α_p given by (22) when $k_1 = 1$. The analytically and numerically calculated cogging torque waveforms for this optimal value of α_p are compared in Fig. 19. It is apparent from (28) and Fig. 19 that the analytical cogging torque solution presented in this paper can be used to accurately calculate α_p for minimum cogging torque in spite of the noticed deviations from finite-element solutions.

D. Other Examples

It can also be shown in some similar examples that this method for calculation of cogging torque, which involves complex relative air-gap permeance and the flux density in the slotless air gap, can equally well capture the effects of other known methods for cogging torque minimization in surface PM motors. Some of these methods are different slot/pole

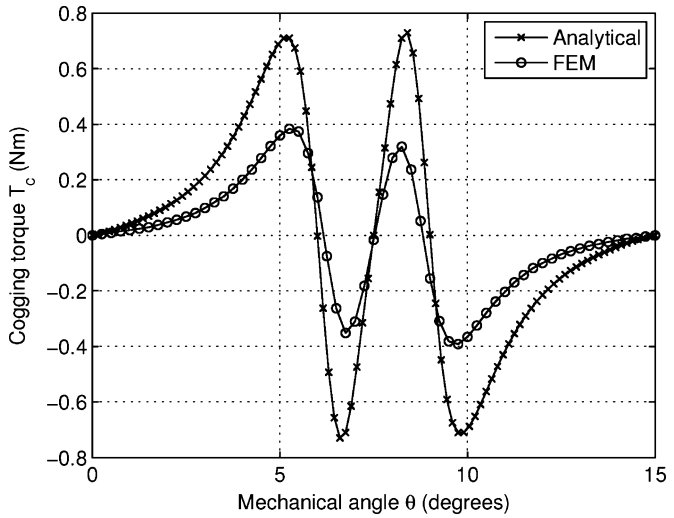

Fig. 19. Comparison of cogging torque waveforms calculated analytically and numerically for the optimal magnet-arc to pole-pitch ratio ($\alpha_p = 0.8452$) which yields minimum cogging torque.

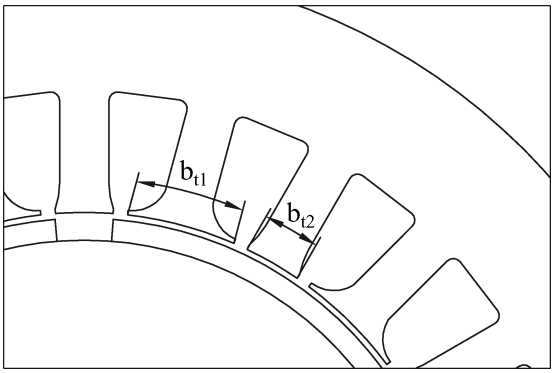

Fig. 20. Cross section of a part of the motor showing slots with shifted slot openings and different tooth widths in the case of teeth pairing.

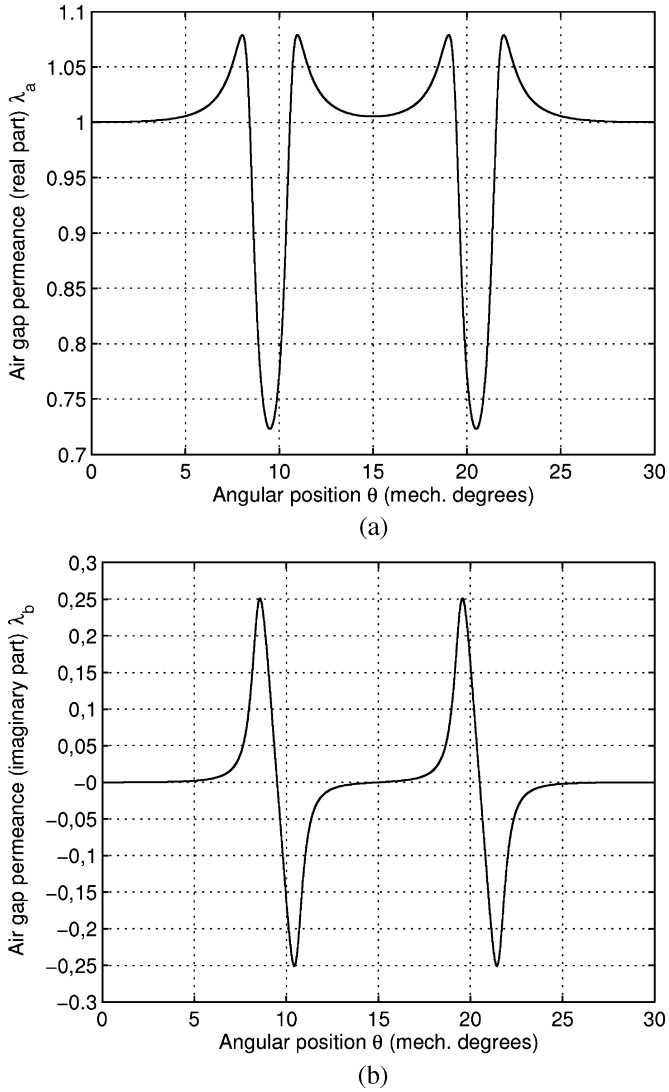

Fig. 21. Waveforms of the complex relative air-gap permeance in the middle of the air gap for two slot pitches in the case of teeth pairing with slot openings shifted by 2^0. (a) Real component. (b) Imaginary component.

combinations including fractional slot windings [20]–[22], adjusting the slot opening width [20], [22], air-gap length and magnet thickness, using different types of magnetization (radial, parallel, etc.) [22], [23], shifting of permanent magnets [24]–[27], notches in the stator teeth [22], [24], [28], [29], teeth pairing [4], [30], slot width pairing [31], magnet segmentation [32], stepped skewing of magnets [22], [24], etc. However, in some of these cases a new equation similar to (21) would have to be derived for calculation of cogging torque.

For example, in the case of teeth pairing (see Fig. 20), the period of the complex relative air-gap permeance is two slot pitches and the widths of the adjacent teeth differ. The air-gap permeance can either be assembled point by point using the solution for a single slot opening presented in this paper, or a more accurate approach would be to calculate the permeance numerically using MATLAB SC Toolbox [33]. The real and imaginary parts of the air-gap permeance calculated using SC toolbox for the case when the slot opening of each slot is shifted by 2° are shown in Fig. 21. The magnet-arc to pole-pitch ratio is $\alpha_p = 0.9$ and the width of the slot opening is $b_o = 2$ mm. For calculation of cogging torque, the Fourier coefficients λ_0, λ_{am}, and λ_{bm} have to be calculated from the waveforms in Fig. 21 using the discrete Fourier transform, and in (21) the number of slots Q_s has to replaced by $Q_s/2$. The analytically and numerically calculated cogging torque waveforms for the case of teeth pairing are compared in Fig. 22. The discrepancies between the waveforms are consistent with the observations made earlier. The Differential Evolution can be used in this case as well to find the optimum magnet-arc to pole-pitch ratio and the shift of the slot openings which yield minimum cogging torque.

V. Conclusion

An analytical solution of the integral of Maxwell stress tensor has been developed for calculation of cogging torque in surface PM motors. The solution is based on utilization of the principle of complex relative air-gap permeance derived from conformal mapping theory which takes into account the presence of slots in the stator of the motor. The method takes into account permanent magnet properties and all relevant geometric parameters of the motor (number of slots and poles, air-gap length, magnet

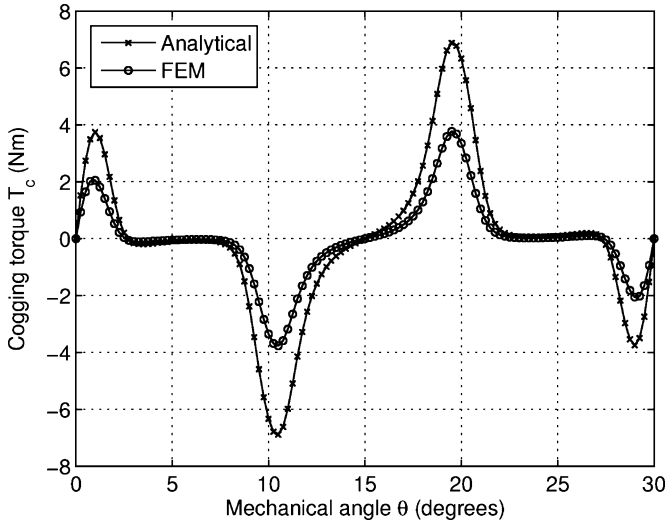

Fig. 22. Comparison of cogging torque waveforms calculated analytically and numerically for the case of teeth pairing with slot openings shifted by 2^0.

dimensions, size and position of the slot openings, etc.) which affect the cogging torque waveform and magnitude.

In comparison with the finite-element solution, the analytical solution yields higher peak values of cogging torque. This discrepancy is caused by spatial distortions due to the logarithmic nature of conformal transformations between complex planes containing different air-gap geometries. Nevertheless, it has been shown in an example that this analytical solution is able to correctly predict the optimal magnet-arc to pole-pitch ratio which yields minimum cogging torque. Using the principle of complex relative air-gap permeance and the flux density solution in the slotless air gap, similar solutions for cogging torque can be derived when employing other methods of cogging torque minimization mentioned in the paper. An example is given for teeth pairing. A method for optimization, like Differential Evolution, combined with this type of cogging torque solution can be used in the design stage to correctly determine the motor geometry which yields minimum cogging torque.

REFERENCES

[1] J. D. L. Ree and N. Boules, "Torque production in permanent-magnet synchronous motors," *IEEE Trans. Ind. Appl.*, vol. 25, no. 1, pp. 107–112, Jan. 1989.

[2] K.-H. Kim, D.-J. Sim, and J.-S. Won, "Analysis of skew effects on cogging torque and BEMF for BLDCM," in *Conf. Rec. 1991 IEEE Ind. Applicat. Soc. Annu. Meeting*, Dearborn, MI, 1991, vol. 1, pp. 191–197.

[3] B. Ackermann, J. H. H. Janssen, R. Sottek, and R. I. Van Steen, "New technique for reducing cogging torque in a class of brushless DC motors," *IEE Proc. B—Electr. Power Appl.*, vol. 139, no. 4, pp. 315–320, Jul. 1992.

[4] S. M. Hwang, J. B. Eom, G.-B. Hwang, W.-B. Jeong, and Y.-H. Yung, "Cogging torque and acoustic noise reduction in permanent magnet motors by teeth pairing," *IEEE Trans. Magn.*, vol. 36, no. 5, pp. 3144–3146, Sep. 2000.

[5] J. F. Gieras, "Analytical approach to cogging torque calculation in PM brushless motors," in *Int. Electr. Machines & Drives Conf.*, Madison, WI, Jun. 2003, vol. 2, pp. 815–819.

[6] C. S. Koh and J.-S. Seol, "New cogging-torque reduction method for brushless permanent-magnet motors," *IEEE Trans. Magn.*, vol. 39, no. 6, pp. 3503–3506, Nov. 2003.

[7] Y. Yang, X. Wang, R. Zhang, T. Ding, and R. Tang, "The optimization of pole arc coefficient to reduce cogging torque in surface-mounted permanent magnet motors," *IEEE Trans. Magn.*, vol. 42, no. 4, pp. 1135–1138, Apr. 2006.

[8] Z. Q. Zhu and D. Howe, "Analytical prediction of the cogging torque in radial-field permanent magnet brushless motors," *IEEE Trans. Magn.*, vol. 28, no. 2, pp. 1371–1374, Mar. 1992.

[9] A. B. Proca, A. Keyhani, A. El-Antably, W. Lu, and M. Dai, "Analytical model for permanent magnet motors with surface mounted magnets," *IEEE Trans. Energy Convers.*, vol. 18, no. 3, pp. 386–391, Sep. 2003.

[10] M. Marković, M. Jufer, and Y. Perriard, "Reducing the cogging torque in brushless DC motors by using conformal mappings," *IEEE Trans. Magn.*, vol. 40, no. 2, pp. 451–455, Mar. 2004.

[11] D. Žarko, D. Ban, and T. A. Lipo, "Analytical calculation of magnetic field distribution in the slotted air gap of a surface permanent-magnet motor using complex relative air-gap permeance," *IEEE Trans. Magn.*, vol. 42, no. 7, pp. 1828–1837, Jul. 2006.

[12] M. Marković, M. Jufer, and Y. Perriard, "Determination of tooth cogging force in a hard-disk brushless DC motor," *IEEE Trans. Magn.*, vol. 41, no. 12, pp. 4421–4426, Dec. 2005.

[13] Z. Q. Zhu and D. Howe, "Instantaneous magnetic field distribution in brushless permanent magnet DC motors, part III: Effect of stator slotting," *IEEE Trans. Magn.*, vol. 29, no. 1, pp. 143–151, Jan. 1993.

[14] X. Wang, Q. Li, S. Wang, and Q. Li, "Analytical calculation of air-gap magnetic field distribution and instantaneous characteristics of brushless DC motors," *IEEE Trans. Energy Convers.*, vol. 18, no. 3, pp. 424–432, Sep. 2003.

[15] U. Kim and D. K. Lieu, "Magnetic field calculation in permanent magnet motors with rotor eccentricity: With slotting effect considered," *IEEE Trans. Magn.*, vol. 34, no. 4, pp. 2253–2266, Jul. 1998.

[16] Z. Q. Zhu, D. Howe, E. Bolte, and B. Ackermann, "Instantaneous magnetic field distribution in brushless permanent magnet dc motors, part I: Open-circuit field," *IEEE Trans. Magn.*, vol. 29, no. 1, pp. 124–135, Jan. 1993.

[17] Z. Haznadar and Ž. Štih, *Elektromagnetizam* (in Croatian). Zagreb: Školska knjiga, 1997, vol. I.

[18] J. Lampinen, "Multi-constrained nonlinear optimization by the differential evolution algorithm," presented at the 6th On-Line World Conf. Soft Comput. Ind. Applicat. (WSC6), Sep. 2001.

[19] D. Žarko, "A systematic approach to optimized design of permanent magnet motors with reduced torque pulsations" Ph. D. dissertation, Univ. Wisconsin, Madison, Sep. 2004 [Online]. Available: http://www.esa.fer.hr/djelatnici/zarko_damirENG.htm

[20] Z. Q. Zhu and D. Howe, "Influence of design parameters on cogging torque in permanent magnet machines," *IEEE Trans. Energy Convers.*, vol. 15, no. 4, pp. 407–412, Dec. 2000.

[21] T. M. Jahns and W. Soong, "Pulsating torque minimization techniques for permanent magnet AC motor drives—A review," *IEEE Trans. Ind. Electron.*, vol. 43, no. 2, pp. 321–330, Apr. 1996.

[22] M. S. Islam, S. Mir, and T. Sebastian, "Issues in reducing the cogging torque of mass-produced permanent-magnet brushless DC motor," *IEEE Trans. Ind. Applicat.*, vol. 40, no. 3, May/Jun. 2004.

[23] Z. Q. Zhu, D. Howe, and C. C. Chan, "Improved analytical model for predicting the magnetic field distribution in brushless permanent-magnet machines," *IEEE Trans. Magn.*, vol. 38, no. 1, pp. 229–238, Jan. 2002.

[24] N. Bianchi and S. Bolognani, "Design techniques for reducing the cogging torque in surface-mounted PM motors," *IEEE Trans. Ind. Appl.*, vol. 38, no. 5, pp. 1259–1265, Sep. 2002.

[25] C. Studer, A. Keyhani, T. Sebastian, and S. K. Murthy, "Study of cogging torque in permanent magnet machines," in *IAS '97. Conf. Rec. 1997 IEEE Ind. Applicat. Conf. Thirty-Second IAS Annu. Meeting*, New Orleans, LA, 1997, vol. 1, pp. 42–49.

[26] C. Breton, J. Bartolome, J. A. Benito, G. Tassinario, I. Flotats, C. W. Lu, and B. J. Chalmers, "Influence of machine symmetry on reduction of cogging torque in permanent-magnet brushless motors," *IEEE Trans. Magn.*, vol. 36, no. 5, pp. 3819–3823, Sep. 2000.

[27] C. A. Borghi, D. Casadei, A. Cristofolini, M. Fabbri, and G. Serra, "Application of a multiobjective minimization technique for reducing the torque ripple in permanent-magnet motors," *IEEE Trans. Magn.*, vol. 35, no. 5, pp. 4238–4246, Sep. 1999.

[28] S. Hwang and D. K. Lieu, "Design techniques for reduction of reluctance torque in brushless permanent magnet motors," *IEEE Trans. Magn.*, vol. 30, no. 6, pp. 4287–4289, Nov. 1994.

[29] R. P. Deodhar, D. A. Staton, and T. J. E. Miller, "Modelling of skew using the flux-mmf diagram," in *Proc. 1996 Int. Conf. Power Electronics, Drives Energy Syst. For Ind. Growth*, 1996, vol. 1, pp. 546–551.

[30] S. M. Hwang, J. B. Eom, Y. H. Jung, D. W. Lee, and B. S. Kang, "Various design techniques to reduce cogging torque by controlling energy variation in permanent magnet motors," *IEEE Trans. Magn.*, vol. 37, no. 4, pp. 2806–2809, Jul. 2001.

[31] Y. Yang, X. Wang, R. Zhang, C. Zhu, and T. Ding, "Research of cogging torque reduction by different slot width pairing permanent magnet motors," in *Proc. 8th Int. Conf. Electr. Machines Syst.*, Nanjing, China, Sep. 27–29, 2005, vol. 1, pp. 367–370.
[32] R. Lateb, N. Takorabet, and F. Meibody-Tabar, "Effect of magnet segmentation on the cogging torque in surface-mounted permanent-magnet motors," *IEEE Trans. Magn.*, vol. 42, no. 3, pp. 442–445, Mar. 2006.
[33] T. A. Driscoll, *Schwarz Christoffel Toolbox Users Guide—Version 2.3* Dept. Mathematical Sciences, Univ. Delaware. Newark, DE, 2002 [Online]. Available: http://www.math.udel.edu/driscoll/SC

Manuscript received May 15, 2006; revised September 17, 2007. Corresponding author: D. Zarko (e-mail: damir.zarko@fer.hr).

Damir Žarko (M'06) was born in Zagreb, Croatia. He received the B.S. and M.S. degrees in electrical engineering from the University of Zagreb in 1995 and 1999, respectively, and the Ph.D. degree from the University of Wisconsin-Madison in 2004.

Currently, he is a Senior Assistant in the Department of Electrical Machines, Drives and Automation, Faculty of Electrical Engineering and Computing, University of Zagreb, Croatia, where his research activities are related to design, modeling, analysis, and optimization of electrical machines.

Drago Ban (M'01) received the B.S., M.S., and Ph.D. degrees in electrical engineering from the Faculty of Electrical Engineering, University of Zagreb, Zagreb, Croatia, in 1965, 1975, and 1987, respectively.

From 1968 to 1989, he worked as a Development and Project Engineer at KONCAR-Electrical Industry, Zagreb, Croatia. He is currently a full Professor in the Department of Electrical Machines, Drives and Automation, Faculty of Electrical Engineering and Computing, University of Zagreb, Croatia. His scientific and professional activities have been related to the field of electrical machinery, electrical drives, and technical diagnostics.

Prof. Ban was the chairman of several international conferences on electrical drives and power electronics: EDPE 1996, EDPE 1998, EDPE 2000, and EPE-PEMC 2002. He is a member of several international professional associations, and a member of the Croatian Academy of Engineering.

Thomas A. Lipo (M'64–SM'71–F'87) was born in Milwaukee, WI. He received the B.E.E. and M.S.E.E. degrees from Marquette University, Milwaukee, WI, in 1962 and 1964, and the Ph.D. degree in electrical engineering from the University of Wisconsin in 1968.

From 1969 to 1979, he was an Electrical Engineer in the Power Electronics Laboratory of Cooperate Research and Development of the General Electric Company, Schenectady, NY. He became Professor of Electrical Engineering at Purdue University, West Lafayette, IN, in 1979, and in 1981 he joined the University of Wisconsin, Madison, in the same capacity, where he is presently the W. W. Grainger Professor for Power Electronics and Electrical Machines.

Dr. Lipo has received the Outstanding Achievement Award from the IEEE Industry Applications Society, William E. Newell Award of the IEEE Power Electronics, and the 1995 Nicola Tesla IEEE Field Award from the Power Engineering Society for his work. He has served IEEE in various capacities, including President of Industrial Applications Society. He is a Fellow of IEE (London), a member of IEE (Japan), and a Fellow of the Royal Academy of Great Britain.